PRECISE DOCKING AT CHARGING STATIONS FOR LARGE-CAPACITY VEHICLES

An Advanced Driver-Assistance System for Drivers of Electric Urban Buses

Maciej Marcin Michałek, Tomasz Gawron, Michał Nowicki, and Piotr Skrzypczyński

xxxxx

Contemporary transportation is developing toward applications of large-capacity vehicles. This trend is caused mainly by environmental and economic factors. In the public transportation area, it leads to the use of long and articulated electric buses, which are difficult to maneuver, even for experienced drivers. Consequently, there is a need to develop advanced driver-assistance systems (ADAS) for operators of urban buses to safely perform positioning maneuvers with acceptable precision. This article presents an ADAS concept dedicated to the task of precisely docking a pantograph tip with a charging station. We describe the functional structure of the ADAS and explain details of its interconnected components responsible for motion algorithmization, environmental perception, and vehicle localization. Experimental results of assisted pantograph docking maneuvers obtained with an articulated electric bus are provided.

Digital Object Identifier 10.1109/MVT.2021.3086979
Date of current version: 7 July 2021

Background

The Need for ADAS in Urban Buses

Two-body, or multibody, electric urban buses (Figure 1) provide a means to solve traffic congestion and air pollution, as they are high-capacity, zero-emission vehicles [1]. However, due to their batteries' limited capacity, they need to be recharged along their routes. Most commonly, an off-board charging station is used, and a bus has to dock a pantograph with the station's head [2]. This task is difficult for drivers, particularly in the case of articulated vehicles. The maneuver can be performed only when moving forward, as reversing is prohibited to ensure safety. Although serious driver mistakes may damage the station's head, even relatively small deviations of the bus trajectory can result in increased pantograph wear. Missing the head leads to repeated docking attempts and results in wasted time and battery power.

Unfortunately, docking stations cannot be replaced by devices that plug into parked vehicles, as in some

electric car charging systems [3]. Bus operators usually do not permit the installation of additional equipment at charging stations due to legal issues and their desire to minimize operating costs. Therefore, they ask bus manufacturers to provide assistive technologies to enable safe and quick docking, even if a driver does not have much experience [4]–[7]. Passive ADAS can solve the problem by providing drivers visual cues, but they do not directly control a vehicle. Functionally, they adhere to Society of Automotive Engineers (SAE) automation level 1 [16]. Hence, ADAS can effectively reduce driver stress, compensate for limited experience, and operate where autonomous vehicles are not permitted in public transportation [5], [6].

This article presents a prototype ADAS for drivers of electric urban buses, which is being cooperatively developed by Poznań University of Technology and European manufacturer Solaris Bus & Coach (SBC). The proposed system builds on and integrates components previously created by the authors in the context of vision-based detection [8] as well as motion planning and feedback control algorithms [9], [10]. The main contribution to the field of intelligent transportation comes from the new concept of the complete ADAS, which adheres to the requirements of bus manufacturers and operators by relying only on onboard sensors and computational systems while being affordable and scalable to various city bus models.

Docking Problem Description

The task of charging station docking can be described with the help of Figure 2. A bus is expected to precisely position a pantograph mounted on its roof against a charging unit that has a known location (which is automatically detected by a perception system). The task can be reformulated as a problem related to the terminal positioning of a specific vehicle guidance point, which is located where it is convenient from the point of view of a motion-control problem. Let us assume that the guidance point is selected as a midpoint of a rear axle (for articulated buses, this corresponds to the second axle from the front). Knowing the geometrical relationship between the pantograph tip and the guidance point, the motion-control problem is to find and execute (in a forward direction) a sufficiently smooth and feasible reference path joining an initial guidance point position (determined by the relative initial locus of the bus with respect to the charging station) with the target location. This guarantees that the pantograph tip will dock with the charger at a prescribed accuracy. The terminal positioning accuracy depends on the pantograph's construction. In practice, it usually admits up to about 0.2 m of Euclidean deviation error, thanks to the self-adaptive tip charger connection (see Figure 1).

Figure 1 An Urbino 18 articulated urban bus, manufactured by SBC, docked with a pantograph at a mockup charging station.

The Concept of ADAS for Urban Buses

The main objective of an ADAS for charging station docking is to compute and update steering commands in real time (using the current state of a vehicle), nominally guiding a bus toward its target while avoiding collisions with known static obstacles. A human–machine interface (HMI) conveys the steering commands to the driver, who is responsible for executing the instructions and for deciding the vehicle's instantaneous forward longitudinal velocity (it is not suggested by the ADAS). Thus, he or she can operate the bus according to his or her skills, ensuring the safety of the vehicle and passengers. Figure 3 illustrates the essential functional blocks of the

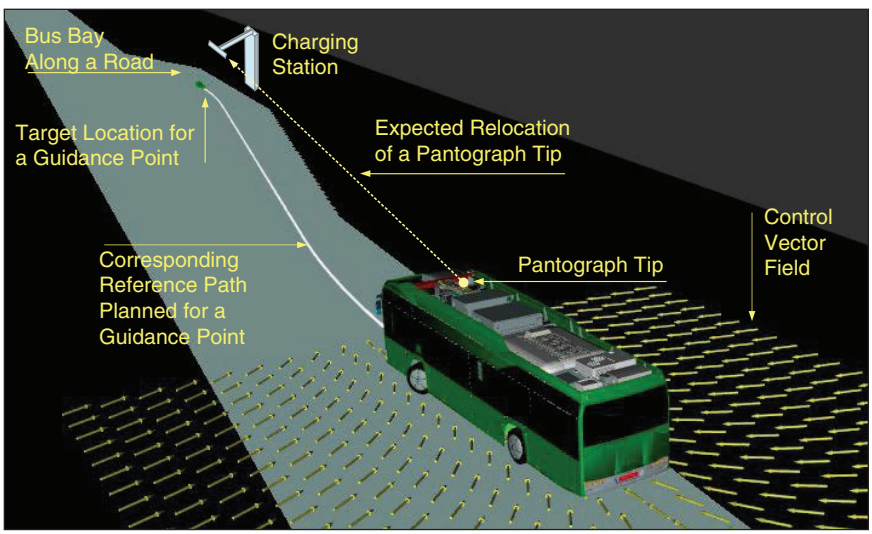

Figure 2 Docking a pantograph tip with a charging station. The control vector field graphically explains the feedback control strategy applied in the proposed ADAS, as discussed in the "Motion Algorithmization Subsystem" section.

proposed ADAS, which can be applied to single-body and articulated buses. The assistance system consists of three underlying functional subsystems:

1) the perception and localization subsystem
2) the motion algorithmization subsystem
3) the interface subsystem.

The system's robustness to imprecise steering command execution is ensured by closing two main feedback loops in a cascade structure, as described in the following:

- the outer feedback loop taken from the estimate $\boldsymbol{q}_E$ of a vehicle's configuration
- the steering feedback loop taken from the current angle β_0 of a vehicle's steering wheel.

The auxiliary inner feedback loop, taken from the joint angle β_1, is used in articulated buses to transform online a wagon's velocity to the prime mover's velocity $\boldsymbol{u}_{0c}$ in a case when a guidance point of the vehicle is located on a wagon's axle.

Perception and Localization Subsystem

For an articulated bus, the charger needs to be detected from a long distance so that the docking maneuver can begin early, considering vehicle kinematics constraints. The perception system consists of sensors linked to onboard computers via Ethernet and USB connections. Standard sensors (such as the tachometer, steering wheel angle encoder, and joint angle encoder) in SBC electric buses are integrated with the system through the controller area network (Figure 4). Lidar sensors are employed to update a simple terrain elevation map, enabling obstacles to be considered while planning and executing maneuvers.

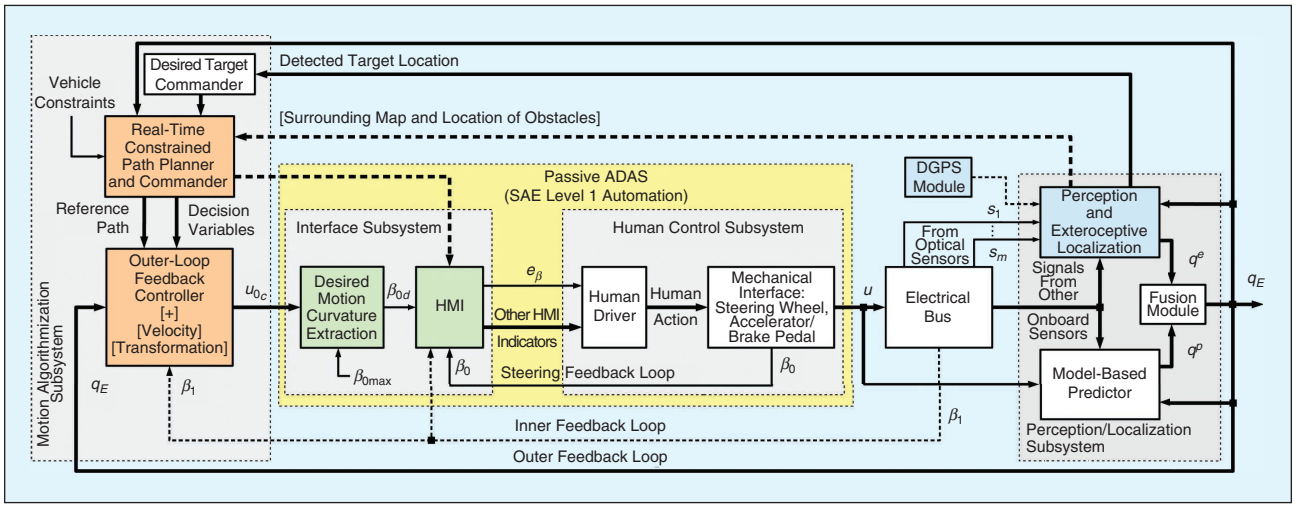

FIGURE 3 The functional block scheme of the proposed ADAS. DGPS: differential GPS.

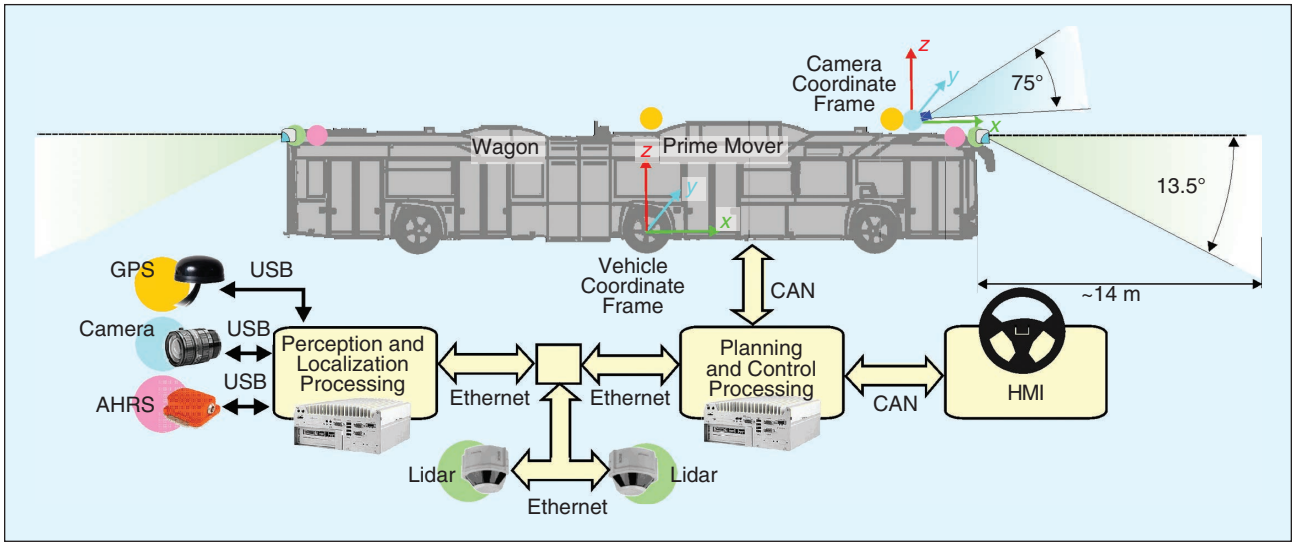

FIGURE 4 The block scheme of the logical and simplified hardware structure of the perception and localization subsystems with connections to other ADAS subsystems (sensor classes are indicated by colors). CAN: controller area network; AHRS: altitude and heading reference system.

The charging station has to be detected, recognized, and localized automatically from a distance up to 30 m. Unfortunately, lidar cannot capture the shape of an object as small as the charging station from that far away. Hence, passive vision is applied for detection and localization. We use a high-resolution (5,472 × 3,648 pixels) camera mounted at the front of the vehicle's roof. The sensing system is enhanced by altitude and heading reference system (AHRS) integrated inertial sensors. Their role is to detect and compensate for unpredictable chassis movements with respect to the reference frame fixed to the axle. The system is completed with two differential GPS (DGPS) receivers. We use two U-blox multiconstellation GPS receivers configured as *rover* and *moving base*, with a third serving as a base station. Correction data are transmitted via an LTE channel. The DGPS makes it possible to obtain the position of each receiver with the nominal accuracy of ±0.01 m in fixed mode, i.e., when a large number of satellites is simultaneously observed and the correction data are received [11]. Having two receivers attached to the roof with a known base distance enables us to compute the yaw angle, which is the orientation of the bus in the external world frame.

If we survey the position of the charging station using the DGPS and ensure that a base station is nearby, we can use the DGPS to guide the docking maneuvers with high accuracy. However, we still want to automatically recognize and detect the charging station from an approaching bus to eliminate failures due to temporarily unavailable GPS signals and differential corrections. Therefore, in [8], we introduced a vision-based recognition system that applies a convolutional neural network (CNN) trained on a data set of example images. Faster region-based CNN (R-CNN) and Mask R-CNN models [12] are employed to detect a bounding box on the charger's head, predict the exact segmentation mask of the charger's head, and determine the head's characteristic points in an image. To ensure real-time operation, we locate the entire charging station on a downsampled image using a Faster R-CNN and define a region of interest (ROI) on the bounding box location provided by the network. Next, we detect the charger's head within the ROI on the full-size image. Applying a learning-based approach, we had to take much care with the preparation of the training data set to have acceptable recognition results while reducing false positives almost to zero. This goal was achieved with the explainable learning concept [8], which enabled us to select proper negative examples (e.g., vehicles, building facades, and glazed panels) to augment the training data set, eventually reducing the number of false charger detection events.

The Mask R-CNN has a mask predictor head, which yields the exact segmentation mask of a detected object. We modified this network by adding a regressor head that finds feature points of the object within the boundaries. To train our network for the detection of feature points, we had to extend the data set of charger images with additional metadata describing the location of the features. The charger head's natural corners were selected as features. It is possible to determine the distance to a known object through a single image, provided that a model of the object is available. We have a CAD model of the charging station, and we use the head's corners indicated on the image by the detected feature points. With this information and the camera calibrated beforehand, we use the iterative SolvePnP algorithm [13] to estimate the six-degrees-of-freedom pose of the charging station's head with respect to the camera coordinate system. The roll and pitch angles of the camera are known from the AHRS; thus, they are ignored in this procedure.

Once the geometric relation between the camera and the charger's coordinate system is known, we can easily obtain the camera pose with respect to the charger and, then, the pose of the guidance point in a vehicle's coordinate system with respect to the charger. This pose can substitute for the one from the DGPS in case of problems with the satellite-based system. The vehicle pose $\boldsymbol{q}_e$ estimated on the exteroceptive localization system is next fused (using a complementary weighted combination) with an estimate $\boldsymbol{q}_p$ from a model-based predictor (Figure 3), which computes a mathematical model of vehicle kinematics response online.

Motion Algorithmization Subsystem

The motion algorithmization subsystem consists of two main parts (highlighted in orange in Figure 3):

- the constrained path planner and commander
- the outer-loop feedback control module.

At the beginning of a docking task, on the driver's command and after the perception subsystem recognizes the charging station, the path planner computes a reference path joining the current configuration of the bus with a target configuration determined by an initial relative location of the charger with respect to the vehicle frame. The planner looks for a path that satisfies the following constraints and optimization criteria [9] (in order of importance):

1) a collision-free path (with respect to known static obstacles and taking into account bus body dimensions)
2) a curvature-limited path (the maximal absolute curvature of the path cannot violate the maximal admissible steering angle $\beta_{0\max}$ of a bus)
3) a sufficiently smooth path (the absolute curvature rate cannot exceed imposed steering rate limitations)
4) a shortest-length path with a minimal number of segments (two-segment paths are preferred, constituting the splines up to a seventh degree).

Thanks to specific properties of the docking maneuver, most of the planning computations are performed

using analytical (geometrical) relations, which helps speed up the planning process. In more complicated cases, the planner numerically searches for the path using the state lattices approach [9], [14], which casts the path-planning problem to a graph-search problem after building an implicit multidimensional grid in the vehicle's configuration space by recursively expanding a predefined set of path primitives. The path computed by the planner is provided in a nonparameterized form by via the so-called level curve approach (see, e.g., [9]), where the equation $F(x, y) = 0$ determines a set of points (x, y) on a plane representing a reference path as an intersection of the surface $F(x, y) = z$ with the plane $z = 0$. The path is expressed in a local frame attached to the currently active segment. The activation of a path segment is performed by the path commander module on the current pose of the bus. An exemplary reference path, found by the constrained planning module for the docking task and satisfying requirements 1)–4) in the preceding, is presented in Figure 2.

When the reference path is ready, the outer loop feedback control module is responsible for computing the prime mover's instantaneous desirable velocity vector $\boldsymbol{u}_{0c}$, which should guide the vehicle along the path toward the target location. The vector $\boldsymbol{u}_{0c}$, consisting of a computed longitudinal velocity v_{0c} for the guidance point and an angular commanded velocity ω_{0c} of the prime mover's body, is updated in real time based on the current value of estimated vehicle configuration $\boldsymbol{q}_E$, using the Vector-Field-Orientation (VFO) path-following (PF) control strategy proposed in [10]. It has been shown that applying the VFO PF control function is relatively intuitive and leads to easily predictable nonoscillatory movement of a vehicle in a transient stage as it is smoothly guided toward, and then along, a reference path. Figure 2 demonstrates the exemplary flow of a control vector field computed by the VFO PF method, which determines a desirable motion curvature for a vehicle in the vicinity of the reference path.

After computing the commanded velocity vector $\boldsymbol{u}_{0c}$, the extraction module (the first left-hand block in

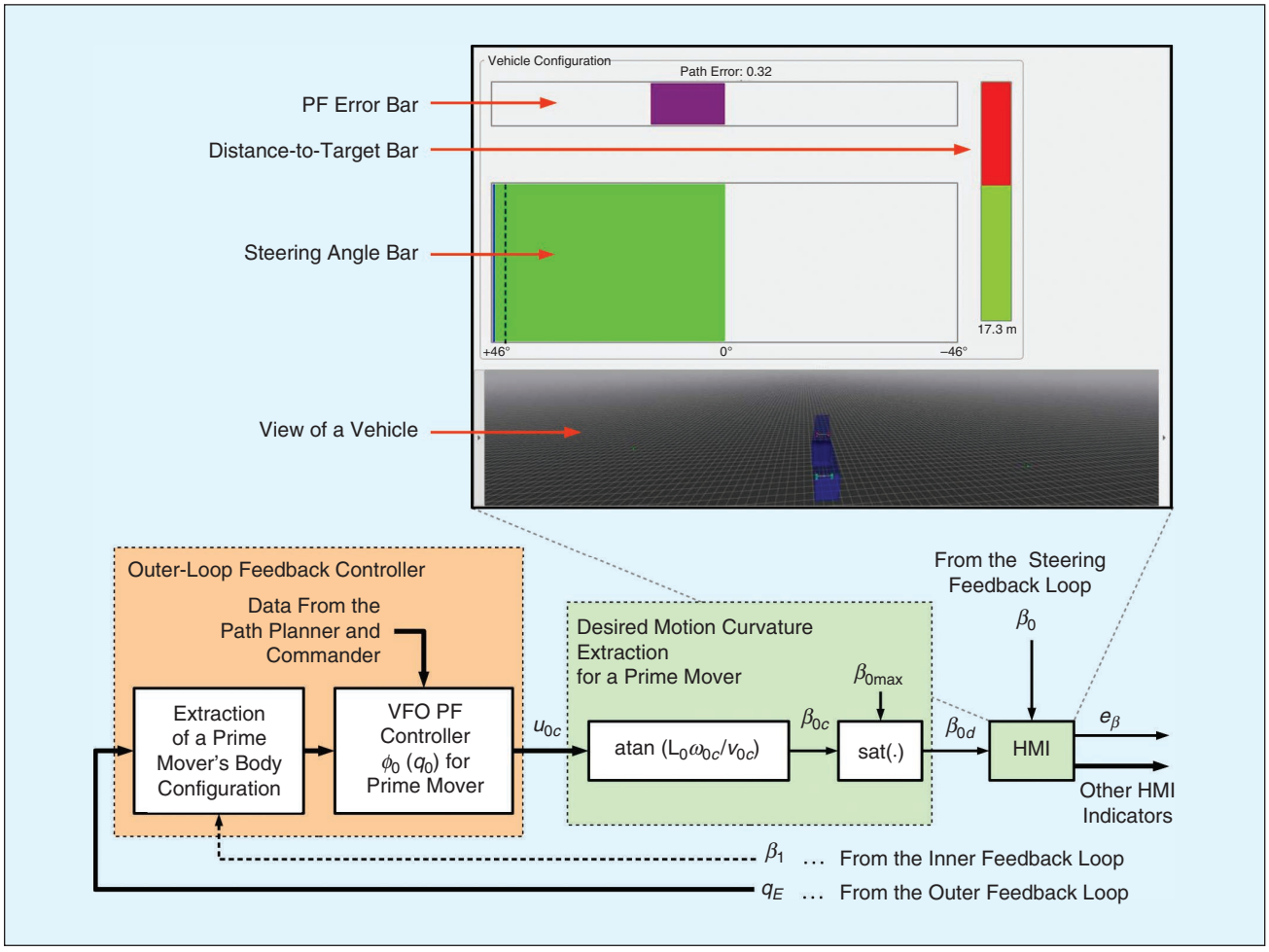

FIGURE 5 Bar indicators and the feedback control (orange) and interface (green) subsystems.

the green area in Figure 5) computes an instantaneous steering angle β_{0c} corresponding to the desired instantaneous motion curvature of the bus, determined by velocity $\boldsymbol{u}_{0c}$. The computed steering angle β_{0c} goes through the saturation block (accounting for the bus's steering angle limitation $\beta_{0\max}$) and is provided to the driver by the HMI. Thanks to the outer feedback loop, the feedback control module is capable of correcting in real time the commanded steering angle to compensate for the resultant PF error when the driver imprecisely follows the instructions.

Interface Subsystem

The interface subsystem (the green blocks in Figures 3 and 5) consists of two functional blocks: the HMI and the block extracting a bus's instantaneous commanded motion curvature, which is proportional to a tangent of the commanded steering angle β_{0c}, saturated to the desired steering angle β_{0d}. To limit driver burdens, we designed a key part of the HMI in a minimalistic form, that is, as a set of three bars on a graphic display (Figure 5; see the video links in the "Maneuvering Results With ADAS" section). The first bar indicates the current PF error, the second one provides the desired (determined on β_{0d}) and current (based on β_0) steering angle values, and the third shows the current distance to a target. The driver is expected to track only the second bar by turning the steering wheel. At present, the HMI is a test solution; its development for real traffic conditions is an open problem that exceeds the scope of this article.

Experimental Results

Automatic Detection and Localization of a Charger

Experiments concerning the perception and localization components of the ADAS were performed with a full-scale mockup of a charging station and by partially using actual charging stations for SBC buses in Warsaw, Poland. Our trials demonstrated that a charging station is reliably detected from a distance of more than 40 m, owing to the high resolution of the acquired images and the learning-based detection procedure, which is robust to false positives. Figure 6 provides an example detection result for a training data set augmented with additional negative examples (green labels) versus a false detection (the red label) generated by a network trained only on positive examples. The attention heat map, where warmer colors denote pixels more likely to belong to the sought class (the charging station's head) and cooler colors represent the neutral background, clearly indicates that the network is focused on the real object.

The vehicle localization accuracy with respect to the charging station was investigated using ground truth obtained from the DGPS. The pose estimate was computed considering learned key points [Figure 7(a)]. A sample

FIGURE 6 An exemplary charger detection result demonstrating the influence of a properly designed training data set with negative examples [8].

mean of errors from 17 maneuvers plotted in Figure 7(b) versus the distance to the charging station demonstrates that the vision-based localization method yields accurate enough results at distances up to 30 m, while the average error is bounded within the 0.1-m value, as required by the path-planning module, for distances shorter than 15 m. This is the stage of the docking scenario when the best accuracy is needed to smoothly plug in the pantograph tip.

Maneuvering Results With ADAS

A series of assisted docking field tests with the ADAS were conducted using an 18-m Urbino 18 Electric bus (Figure 1). An SBC employee drove the vehicle. Human factors (i.e., the performance of drivers with different ages and experience) were not considered, as the prototype was tested only in an emulated operational environment (achieving the sixth level of technological readiness). A study of human factors will occur during trials in a fully operational environment. The bus was equipped with a steering wheel angle sensor, a joint angle sensor, and two DGPS antennas mounted on the roof above the first two axles. The antennas delivered the body's position and orientation in real time at a frequency of 10 Hz. The best static measurement of their position was roughly ±0.027 m (a standard deviation). Commands computed by the ADAS and provided to the driver were updated at an average frequency of about 100 Hz. The pantograph was mounted on the roof just above the front (steering) axle. The docking maneuver, in the first stage, required positioning a characteristic bus point (i.e., the midpoint of the front axle) at a target location and, in the second stage, unfolding the pantograph to contact the charger.

A series of 27 tests was conducted in an almost obstacle-free parking space, with the mockup charging station (see Figure 1). These trials were different than those used to assess the accuracy of the vision-based

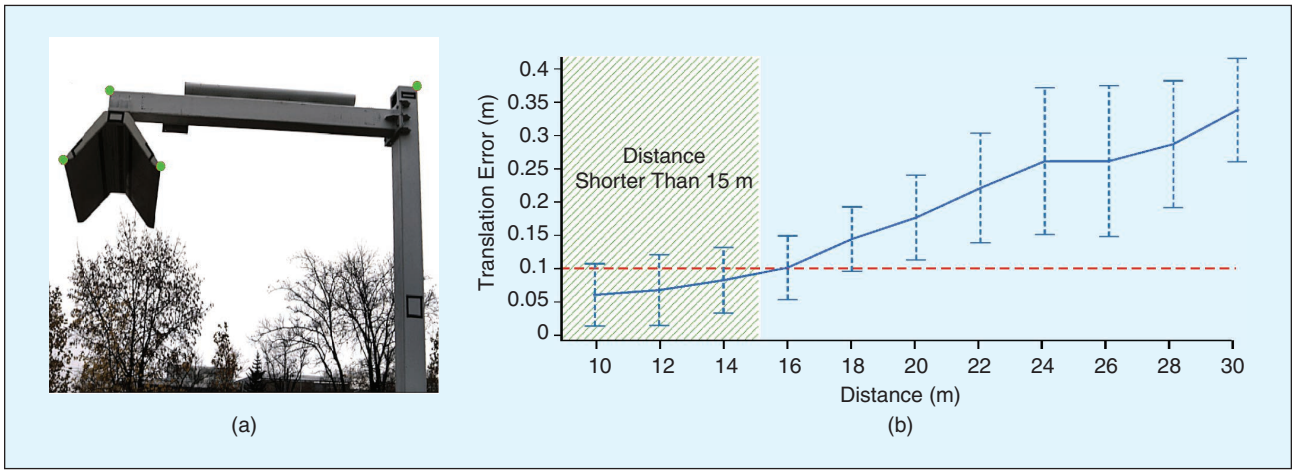

FIGURE 7 The charging station localization accuracy demonstrated through the distance between the camera and the station's head versus the DGPS ground truth. (a) The detected key points. (b) The sample mean of the measured distance error, with the standard deviation.

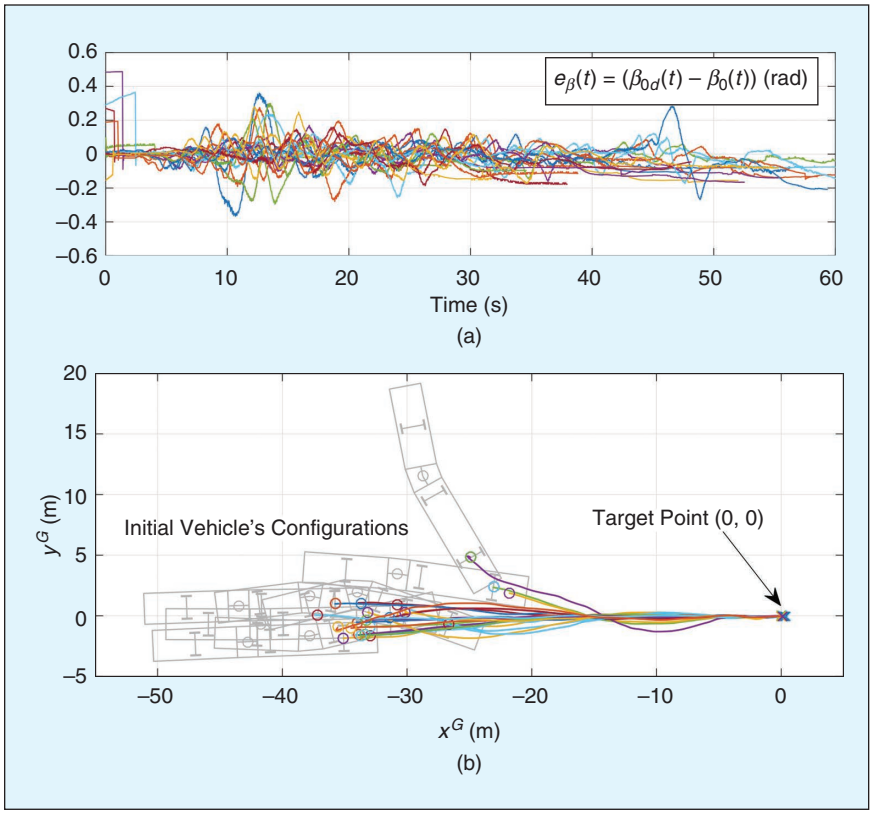

FIGURE 8 The results of 24 docking field tests using the proposed ADAS. (a) The steering errors e_β. (b) The paths drawn by the bus. Eight initial bus configurations have been included.

localization, as the data logged in the experiments were dissimilar. For every test, the driver had to perform a maneuver from a different (sometimes difficult) initial configuration to verify the efficiency of the ADAS. Among the trials, 24 were successful, with the best average positional accuracy no worse than 0.1 m (the Euclidean metric). Three trials failed due to very hard initial conditions (the DGPS antennas were occluded by a tall building). Because the two bus localization subsystems (i.e., the DGPS and vision ones) were separately configured and tested, it was not possible to automatically switch to camera mode when the DGPS was unavailable (in the camera localization mode, the same DGPS was used only to collect the ground truth).

A set of results obtained with the ADAS appears in Figure 8. The figure presents time plots of steering errors and the resulting paths drawn by the characteristic point of the bus while maneuvering from various initial configurations to the target point (0,0) (to maintain clarity, only eight representative configurations are drawn). From the evolution of steering errors, one can observe that even for relatively poor driver tracking accuracy (with respect to the ADAS commands), the docking maneuver can be successfully accomplished. This means that the driver's best tracking accuracy is expected in the final stage of the docking maneuver.

The quantitative results, averaged across the successful 24 trials, are given in the following (sample mean ± standard deviation):

- (0.053 ± 0.025) m for the minimal distance of the characteristic point to the target location during maneuvering
- (0.161 ± 0.104) m for the final distance (i.e., after the driver stops the bus) of the characteristic point to the target location

- (0.026 ± 0.006) rad for the prime mover's absolute orientation error at the minimal distance to the target
- (0.028 ± 0.006) rad for the prime mover's absolute orientation error at the final distance to the target.

The minimal and final distances differ mainly because the driver generally stopped the bus along the x^G direction with less care than when positioning the bus laterally with respect to the y^G-axis (the final coordinates along the x^G- and y^G-axes belonged, respectively, to the ranges [–0.049;0.373] m, with a mean of 0.12 m and a standard deviation of 0.142 m, and [–0.091;0.036] m, with a mean of –0.036 m and a standard deviation of 0.031 m). Noticeable differences among the distances were probably caused by several factors affecting the driver, such as the mechanical structure of the charging station's head, which admitted larger positioning errors, and perception limitations resulting from the need to monitor the HMI and the surroundings. Readers can watch videos of the two trials at https://www.youtube.com/watch?v=66Zm8jyhmdk and https://www.youtube.com/watch?v=rXxaZUNe8dA.

Conclusions

The proposed ADAS is a fully passive solution. However, one can classify it within the SAE level 1 automation class since the whole vehicle guidance strategy is computed, updated online, and suggested by the system. We expect that the vision-based localization module can provide the essential redundancy to replace satellite-based position estimates whenever integrity anomalies in the DGPS are detected and prevent the system from being used due to signal blockages, multipath interference, and other reasons. The low-cost monocular configuration and lack of any additional charger infrastructure should increase the acceptance of this solution in practical applications. However, localization without the DGPS at night and in adverse weather conditions (such as heavy rain and snow) remains an open problem. A possible solution is to apply active yet unobtrusive markers on charging stations.

While we have successfully tested the motion algorithmization subsystem and the vision-based localization module for a variety docking maneuver initial configurations (i.e., bus poses), we are aware that other factors can cause failure, such as another large vehicle suddenly occluding the camera view. Hence, if there are no proper input data to the ADAS system, an error can be indicated to the driver, who should continue the maneuver by steering without cues or stop if the situation is dangerous. Moreover, the accuracy of the ADAS-assisted maneuver depends on drivers precisely tracking the HMI cues. Currently, the system's main limitation is the graphic interface, which may burden and distract drivers in some conditions. Designing a more convenient HMI, e.g., by providing the cues through a display on the windshield or using a multimodal HMI with sounds and vibrations, is an open challenge [15].

Acknowledgments

We thank our colleagues Dr. Marcin Kiełczewski, Krzysztof Ćwian, Mateusz Mydlarz, Tomasz Nowak, and Iman Esfandiyar for their help with software development and technical work. The cooperation of Solaris Bus & Coach is highly appreciated. This research is part of the project Advanced Driver Assistance System (ADAS) for Precision Maneuvers With Single-Body and Articulated Urban Buses, cofinanced by the European Union through the European Regional Development Fund within the Smart Growth Operational Program 2014–2020 (contract POIR.04.01.02-00-0081/17-01).

Author Information

Maciej Marcin Michałek (maciej.michalek@put.poznan.pl) is an associate professor at the Institute of Automatic Control and Robotics, Poznań University of Technology (PUT), Poznań, 60-965, Poland, and chair of the Polish Chapter of the IEEE Robotics and Automation Society (2020–2022). He received his Ph.D. and D.Sc. degrees in automatic control and robotics from PUT in 2006 and 2015, respectively. He is a Senior Member of IEEE.

Tomasz Gawron (tomasz.gawron@put.poznan.pl) is a research assistant at the Institute of Robotics and Machine Intelligence, Poznań University of Technology (PUT), Poznań, 60-965, Poland. He received his Ph.D. degree in automatic control and robotics from PUT in 2019. He is a Member of IEEE.

Michał Nowicki (michal.nowicki@put.poznan.pl) is a research assistant professor at the Institute of Robotics and Machine Intelligence, Poznań University of Technology (PUT), Poznań, 60-965, Poland. He received his Ph.D. degree, with honors, in robotics from PUT in 2018. He is a Member of IEEE.

Piotr Skrzypczyński (piotr.skrzypczynski@put.poznan.pl) is a professor at the Institute of Robotics and Machine Intelligence (IRIM), Poznań University of Technology (PUT), Poznań, 60-965, Poland. He is also head of the IRIM Robotics Division, and he leads the IRIM Mobile Robotics Lab. He received his Ph.D. and D.Sc. degrees in robotics from PUT in 1997 and 2007, respectively. He is a Member of IEEE.

References

[1] B. Hemily and R. D. King, "Uses of higher capacity of buses in transit service", Transportation Research Board, Washington, D.C., 2008. [Online]. Available: https://www.nap.edu/catalog/13919/uses-of-higher-capacity-buses-in-transit-service

[2] R. Deng, Y. Liu, W. Chen, and H. Liang, "A survey on electric buses: Energy storage, power management, and charging scheduling," *IEEE Trans. Intell. Transp. Syst.*, vol. 22, no. 1, pp. 9–22, 2021. doi: 10.1109/TITS.2019.2956807.
[3] P. Petrov, C. Boussard, S. Ammoun, and F. Nashashibi, "A hybrid control for automatic docking of electric vehicles for recharging," in *Proc. IEEE Int. Conf. Robot. Automation*, Saint Paul, 2012, pp. 2966–2971.
[4] J. Huang and H.-S. Tan, "Control system design of an automated bus in revenue service," *IEEE Trans. Intell. Transp. Syst.*, vol. 17, no. 10, pp. 2868–2878, 2016. doi: 10.1109/TITS.2016.2530760.
[5] E. Uhlemann, "'Trusting autonomous vehicles', connected and automated vehicles," *IEEE Veh. Tech. Mag.*, vol. 14, no. 2, pp. 121–124, June 2019. doi: 10.1109/MVT.2019.2905521.
[6] K. Bengler, K. Dietmayer, B. Farber, M. Maurer, C. Stiller, and H. Winner, "Three decades of driver assistance systems: Review and future perspectives," *IEEE Intell. Transp. Sys. Mag.*, vol. 6, no. 4, pp. 6–22, 2014. doi: 10.1109/MITS.2014.2336271.
[7] K. Kivekäs, A. Lajunen, F. Baldi, J. Vepsäläinen, and K. Tammi, "Reducing the energy consumption of electric buses with design choices and predictive driving," *IEEE Trans. Veh. Technol.*, vol. 68, no. 12, pp. 11,409–11,419, 2019. doi: 10.1109/TVT.2019.2936772.
[8] T. Nowak, M. Nowicki, K. Ćwian, P. Skrzypczyński, "How to improve object detection in a driver assistance system applying explainable deep learning," in *Proc. IEEE Intell. Veh. Symp. (IV)*, Paris, France, 2019, pp. 26–231.
[9] T. Gawron, M. Mydlarz, M. M. Michałek, "Algorithmization of constrained monotonic maneuvers for an advanced driver assistant system in the intelligent urban buses," in *Proc. 2019 IEEE Intell. Veh. Symp. (IV)*, Paris, France, pp. 218–224.
[10] M. M. Michałek and T. Gawron, "VFO path following control with guarantees of positionally constrained transients for unicycle-like robots with constrained control input," *J. Intell. Robot. Syst.*, vol. 89, nos. 1–2, pp. 191–210, 2018. doi: 10.1007/s10846-017-0482-0.
[11] N. Zhu, J. Marais, D. Betaille, and M. Berbineau, "GNSS position integrity in urban environments: A review of literature," *IEEE Trans. Intell. Transp. Syst.*, vol. 19, no. 9, pp. 2762–2778, 2018. doi: 10.1109/TITS.2017.2766768.
[12] K. He, G. Gkioxari, P. Dollar, R. Girshick, "Mask R-CNN," in *Proc. IEEE Int. Conf. Comput. Vision (ICCV)*, Venice, Italy, 2017, pp. 2980–2988.
[13] R. I. Hartley and A. Zisserman, *Multiple View Geometry in Computer Vision*. Cambridge, U.K.: Cambridge Univ. Press, 2004.
[14] M. Pivtoraiko, R. A. Knepper, and A. Kelly, "Differentially constrained mobile robot motion planning in state lattices," *J. Field Robot.*, vol. 26, no. 3, pp. 308–333, 2009. doi: 10.1002/rob.20285.
[15] A. Özgür Yöntem, K. Li, D. Chu, V. Meijering, and L. Skrypchuk, "Prospective immersive human-machine interface for future vehicles: Multiple zones turn the full windscreen into a head-up display," *IEEE Veh. Technol. Mag.*, vol. 16, no. 1, pp. 1–10, 2020. doi: 10.1109/MVT.2020.3013832.
[16] J. Shuttleworth. "SAE standards news: J3016 automated-driving graphic update." SAE. https://www.sae.org/news/2019/01/sae-updates-j3016-automated-driving-graphic (accessed June 9, 2021).

VT